JACS
JOURNAL OF THE AMERICAN CHEMICAL SOCIETY
Article
pubs.acs.org/JACS

Stable Tetrabenzo-Chichibabin's Hydrocarbons: Tunable Ground State and Unusual Transition between Their Closed-Shell and Open-Shell Resonance Forms

Zebing Zeng,[†] Young Mo Sung,[‡] Nina Bao,[§] Davin Tan,[∥] Richmond Lee,[∥] José L. Zafra,[⊥] Byung Sun Lee,[‡] Masatoshi Ishida,[‡] Jun Ding,[§] Juan T. López Navarrete,[⊥] Yuan Li,[†] Wangdong Zeng,[†] Dongho Kim,*[,‡] Kuo-Wei Huang,*[,∥] Richard D. Webster,*[,#] Juan Casado,*[,⊥] and Jishan Wu*[,†,▽]

[†]Department of Chemistry, National University of Singapore, 3 Science Drive 3, 117543, Singapore

[‡]Spectroscopy Laboratory for Functional π-Electronic Systems and Department of Chemistry, Yonsei University, Seoul 120-749, Korea

[§]Department of Materials Science & Engineering, National University of Singapore, 119260, Singapore

[∥]Division of Chemical and Life Sciences and Engineering and KAUST Catalysis Center, King Abdullah University of Science and Technology (KAUST), Thuwal 23955-6900, Saudi Arabia

[⊥]Department of Physical Chemistry, University of Malaga, Campus de Teatinos s/n, 229071 Malaga, Spain

[#]Division of Chemistry & Biological Chemistry, School of Physical & Mathematical Sciences, Nanyang Technological University, 21 Nanyang Link, 637371, Singapore

[▽]Institute of Materials Research and Engineering, A*Star, 3 Research Link, 117602, Singapore

Supporting Information

ABSTRACT: Stable open-shell polycyclic aromatic hydrocarbons (PAHs) are of fundamental interest due to their unique electronic, optical, and magnetic properties and promising applications in materials sciences. Chichibabin's hydrocarbon as a classical open-shell PAH has been investigated for a long time. However, most of the studies are complicated by their inherent high reactivity. In this work, two new stable benzannulated Chichibabin's hydrocarbons **1-CS** and **2-OS** were prepared, and their electronic structure and geometry in the ground state were studied by various experiments (steady-state and transient absorption spectra, NMR, electron spin resonance (ESR), superconducting quantum interference device (SQUID), FT Raman, X-ray crystallographic etc.) and density function theory (DFT) calculations. **1-CS** and **2-OS** exhibited tunable ground states, with a closed-shell quinoidal structure for **1-CS** and an open-shell biradical form for **2-OS**. Their corresponding excited-state forms **1-OS** and **2-CS** were also chemically approached and showed different decay processes. The biradical **1-OS** displayed an unusually slow decay to the ground state (**1-CS**) due to a large energy barrier (95 ± 2.5 kJ/mol) arising from severe steric hindrance during the transition from an orthogonal biradical form to a butterfly-like quinoidal form. The quick transition from the quinoidal **2-CS** (excited state) to the orthogonal biradicaloid **2-OS** (ground state) happened during the attempted synthesis of **2-CS**. Compounds **1-CS** and **2-OS** can be oxidized into stable dications by $FeCl_3$ and/or concentrated H_2SO_4. The open-shell **2-OS** also exhibited a large two-photon absorption (TPA) cross section (760 GM at 1200 nm).

I. INTRODUCTION

Open-shell polycyclic aromatic hydrocarbons (PAHs) refer to a type of hydrocarbons with one or more than one π-electrons that are not tightly paired into the bonding molecular orbital in the ground state, which is different from the typical PAHs with a closed-shell electronic structure. Open-shell PAHs are of fundamental importance in understanding the nature of chemical bonding and the basic chemical and physical phenomena of π-conjugated systems. Recent experimental and theoretical studies have revealed that open-shell PAHs could show unique electronic, optical, and magnetic properties and thus have promising applications in materials science.[1] In the case of biradical PAHs, the two unpaired or weakly bonded electrons can be either in a low-spin singlet or in a high-spin triplet state. The substances with a singlet ground state can exhibit paramagnetic property via a thermally excited transition from singlet to triplet state if the singlet−triplet energy gap (ΔE_{S-T}) is sufficiently small.[2] Open-shell PAHs with intermediate biradical characters are theoretically predicted to

Received: May 24, 2012
Published: August 14, 2012

dx.doi.org/10.1021/ja3050579 | J. Am. Chem. Soc. 2012, 134, 14513−14525

have enhanced second hyperpolarizability and a large two-photon absorption (TPA) cross section as compared to the corresponding closed-shell and pure diradical systems,[3] and this has been experimentally proven by several open-shell singlet molecules such as Kubo's bisphenalenyls[4] and Osuka's *meso*-diketo hexaphyrin.[5] Therefore, open-shell PAHs could be used as new efficient nonlinear optical (NLO) chromophores for future photonics applications such as optical switching, three-dimensional memory, optical limiting, and photodynamic therapy.[6] Open-shell PAHs usually also exhibit multiple-stage amphoteric redox behavior, which makes them promising materials for low threshold-voltage ambipolar field effect transistors[7] and energy storage devices (e.g., lithium ion batteries).[8] In addition, certain open-shell PAHs can be regarded as graphene nanoflakes with unique magnetic properties and have potential applications for organic spintronics.[9]

Despite all of their intriguing properties and promising applications, the open-shell nature of these molecules has rendered them vulnerable to degradation reactions; therefore, instability remains a key obstacle for their practical applications. Recent progress in synthetic method has led to the successful synthesis and characterization of several types of stable open-shell PAHs: (1) *o*-quinodimethane[10] and *p*-quinodimethane derivatives;[11] (2) phenalenyls,[12] bisphenalenyl[13] and trisphenalenyls;[14] (3) teranthene;[15] and (4) zethrenes.[16] In most cases, both thermodynamic stabilization by π-electron delocalization and kinetic stabilization by blocking of the most reactive sites carrying high-spin density are necessary to obtain stable materials.

Among various known open-shell PAHs, Chichibabin's hydrocarbon possessing a characteristic resonance structure between a closed-shell quinonoid form and an open-shell biradical (Chart 1) has been most extensively studied regarding its ground-state electronic structure and physical properties.[17] Because of the recovery of two aromatic sextet rings in the biradical form, the Chichibabin's hydrocarbon exhibits large biradical character in the ground state. However, Chichibabin's hydrocarbon reacts avidly with oxygen, yielding polymeric peroxide. In addition, it also tends to dimerize and oligomerize to give paramagnetic species. All of these make it challenging to offer a clear-cut conclusion on its ground-state electronic structure.[18] Although some derivatives of Chichibabin's hydrocarbons have been prepared,[19] side reactions such as oxidation, dimerization, polymerization, and decomposition usually cannot be avoided due to the high chemical reactivity of unpaired electrons. Therefore, great attention has been focused on synthesizing and studying long lifetime and stable Chichibabin's hydrocarbons.[20]

Chart 1. Resonance Structures of Chichibabin's Hydrocarbon, Tetrabenzo-Chichibabin's Hydrocarbons, and Its Derivatives 1-CS/1-OS and 2-CS/2-OS

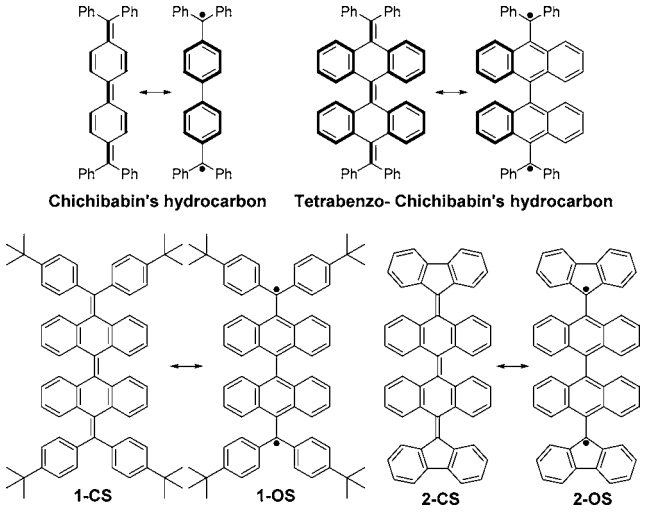

Like other open-shell PAHs, the stabilization of the highly reactive Chichibabin's hydrocarbon can be achieved by either a thermodynamic approach (aromatic stabilization and π-electron delocalization) or kinetic means (steric protection), or by both approaches. As shown in Chart 1, our new strategy toward thermodynamic stabilization of the Chichibabin's hydrocarbon is by benzannulation of the central biphenyl unit with four aromatic benzene rings, and thus tetrabenzo-Chichibabin's hydrocarbon is generated. Such a design can possibly also enhance the kinetic stability due to the steric blocking by the two anthracene units in the case that the biradical form dominates its ground state. Therefore, the tetrabenzo-Chichibabin's hydrocarbon is expected to be more stable due to compensation by both thermodynamic and kinetic stabilization. To improve its solubility and also to further block the reactive sites where dimerization can happen, *tert*-butyl groups are introduced onto the *para*-position of the four phenyl rings in **1-CS**/**1-OS** (Chart 1). It will be of interest to study the inherent electronic structure of this novel hydrocarbon, which can be drawn as a resonance structure between a quinoidal form (**1-CS**) and an open-shell biradical form (**1-OS**). In addition, it has been reported that the stability of a radical center can be improved by delocalization through a fluorenyl moiety.[21] Thus, herein the di(4-*tert*-butylphenyl)-methene groups in **1-CS**/**1-OS** are further replaced by two fluorenyl units, and the obtained molecule can also be drawn as a closed-shell quinoidal form (**2-CS**) or an open-shell biradical (**2-OS**) (Chart 1). The interesting question is whether such substitution will change the ground-state electronic structure of the tetrabenzo-Chichibabin's hydrocarbon. Moreover, considering the large steric hindrance arising from the two anthracene units, the geometric structures of both compounds are also of interest, which could be significantly different from the flat geometry of the parent Chichibabin's hydrocarbon.[17c] In this Article, we report the detailed studies on their synthesis, their ground-state electronic and geometric structures, and transition between their closed-shell and open-shell resonance forms by various experiments assisted by theoretical calculations. Their redox behavior and oxidized species were also investigated. In particular, the dication of the fluorenyl-containing tetrabenzo-Chichibabin's hydrocarbon **2-CS**/**2-OS** provides a new candidate for a study on charged antiaromatic species.[22] In addition, transient absorption and two-photon absorption measurements were conducted to further understand the photophysical properties and NLO response of these types of possibly open-shell hydrocarbons.

II. RESULTS AND DISCUSSION

Synthesis and Structural Characterization of 1-CS/1-OS. The synthetic route toward **1-CS**/**1-OS** is shown in Scheme 1. Treatment of the bianthraquinone **3**[23] with CBr_4/PPh_3 afforded the 11,11,11′,11′-tetrabromo-10,10-bianthraquinodimethane **4** in 90% yield. Subsequently, the tetrabenzo-Chichibabin's hydrocarbon, 11,11,11′,11′-tetrakis(4-*tert*-butyl-

dx.doi.org/10.1021/ja3050579 | J. Am. Chem. Soc. 2012, 134, 14513−14525

Scheme 1. Synthesis of Compound 1-CS and Generation of Its Intermediate Biradical 1-OS[a]

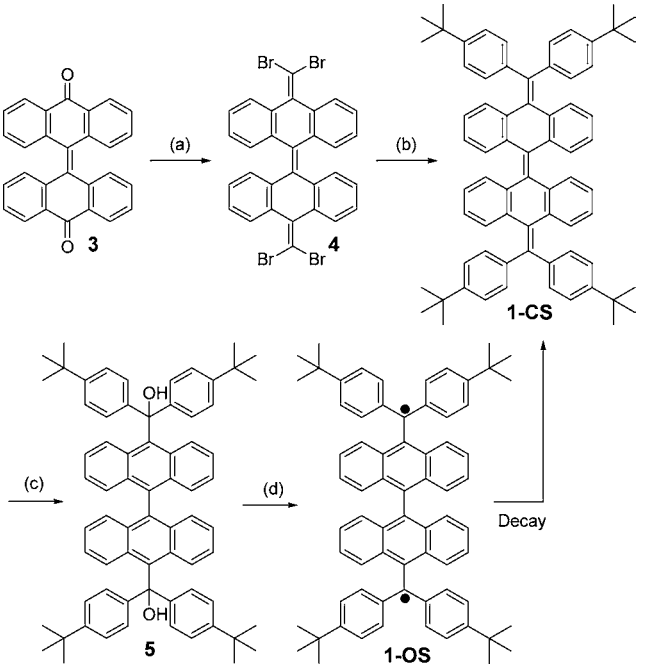

[a]Reaction conditions: (a) CBr_4, PPh_3, toluene, reflux, 36 h, 90%; (b) 4-*tert*-butylphenylboronic acid, $Pd(PPh_3)_4$, Cs_2CO_3–K_2CO_3, toluene/H_2O/EtOH, reflux, 48 h, 90%; (c) DDQ/CH_3SO_3H, CH_2Cl_2, room temperature, 12 h, 75%; (d) $SnCl_2$, dichloromethane, nearly quantitative yield from **5** to **1-OS**.

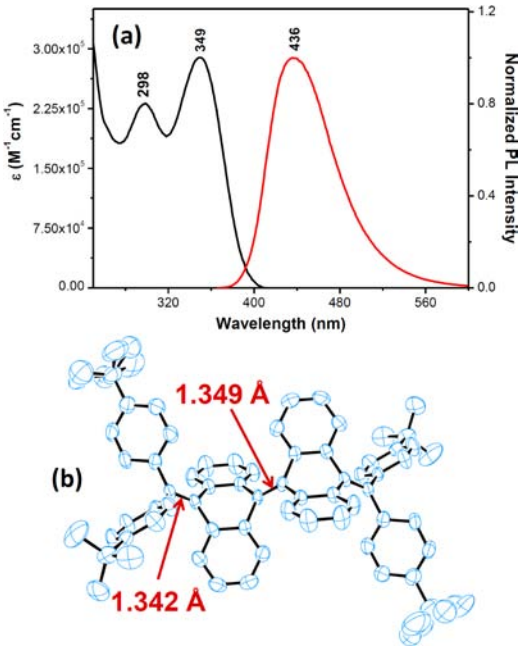

Figure 1. (a) UV–vis absorption spectrum and normalized emission spectrum of compound **1-CS** in DCM. (b) ORTEP plot of the single-crystal structure of **1-CS** with part of the C=C bond labeled with length.

phenyl)-10,10-bianthraquinodimethane (**1-CS**), was conveniently synthesized as a white solid in 90% yield by a 4-fold Suzuki coupling reaction between 4-*tert*-butylphenylboronic acid and the intermediate bromide **4**. Careful choice of the catalyst ($Pd(PPh_3)_4$) and base (a mixture of Cs_2CO_3 and K_2CO_3) was essential to achieve a clean and high-yield reaction.

The steady-state absorption and emission spectra of compound **1-CS** in dichloromethane (DCM) are shown in Figure 1a. Compound **1-CS** displays an intense absorption band in the UV–visible region with absorption maximum at 349 nm (log ε = 5.54; ε: molar extinction coefficient in M^{-1} cm^{-1}), along with a shoulder absorption at 298 nm. Such a band structure is similar to that for the known bisanthraquinone,[24] indicating that the molecule likely has a closed-shell ground state as do normal acenequinones. Compound **1-CS** shows a broad emission band with emission maximum at 436 nm, with a fluorescence quantum yield of 12%. **1-CS** also exhibited clear and sharp ^1H NMR resonances at room temperature even at elevated temperatures (e.g., 100 °C), which further confirmed its closed-shell structure in the ground state. Single crystals were grown by slow diffusion of methanol into a solution of **1-CS** in DCM at room temperature. X-ray crystallographic analysis revealed that **1-CS** existed in a highly contorted, quinoidal structure (Figure 1b).[25] The lengths of the exo methylene bond and the bond between the two anthracene units, as labeled in Figure 1b, are 1.342 and 1.349 Å, respectively, which are quite close to those in typical olefins (1.33–1.34 Å). Thus, there is no doubt that **1-CS** is a closed-shell species. In contrast to the planar geometry observed for the parent Chichibabin's hydrocarbon from its X-ray crystallographic structure,[17c] the central bisanthracene units in **1-CS** are highly twisted due to steric repulsion, and the four additional benzene rings attached to the biphenyl center behave like the wings of a butterfly; thus, the whole molecule looks like a butterfly in the crystal state. The closed-shell ground-state structure of **1-CS** can be ascribed to the loss of two aromatic sextet rings when converted from a quinoidal form to a biradical form (shown in Chart 1), which makes the quinoidal form thermodynamically more stable.

Our intention was to conduct an intramolecular oxidative cyclodehydrogenation reaction of **1-CS** so that a fused, more conjugated hydrocarbon can be generated. The ring cyclization reaction was performed under the well-developed conditions using $FeCl_3$[26] or the 2,3-dichloro-5,6-dicyano-1,4-benzoquinone (DDQ)/CH_3SO_3H system[27] in DCM. Interestingly, no desired ring-closed or even partially cyclized product was found. Alternatively, an unexpected diol **5** was separated in good yield after quenching the reaction with saturated sodium bicarbonate (Scheme 1). This unexpected result indicated that the Scholl-type reaction of **1-CS** when treated with DDQ/H^+ or $FeCl_3$ predominantly generated its dication likely at the exo methylene sites, which is stabilized by charge delocalization through the two phenyl rings and the anthracene units (vide infra). Thus, quenching of the dication with water afforded the diol **5**. The biradical **1-OS** then can be easily generated in nearly quantitative yield by reduction of the diol **5** with $SnCl_2$ in various solvents (e.g., toluene, chloroform, DCM, THF, etc.) (Scheme 1), and MALDI-TOF mass spectroscopy revealed the loss of two –OH groups after reduction. Interestingly, the biradical **1-OS** turned out to be an unstable intermediate, and it relaxed back to the ground-state quinoidal form **1-CS** at an unusually slow rate, which will be discussed in detail in the next section.

Unusually Slow Decay from Open-Shell 1-OS to Closed-Shell 1-CS. The freshly generated biradical **1-OS** by reduction of **5** with excess $SnCl_2$ in toluene displayed a broad

dx.doi.org/10.1021/ja3050579 | J. Am. Chem. Soc. 2012, 134, 14513–14525

long-wavelength absorption band between 680 and 1050 nm with maximum at 834 nm, together with a strong absorption band centered at 507 nm (Figure 2a). This long-wavelength

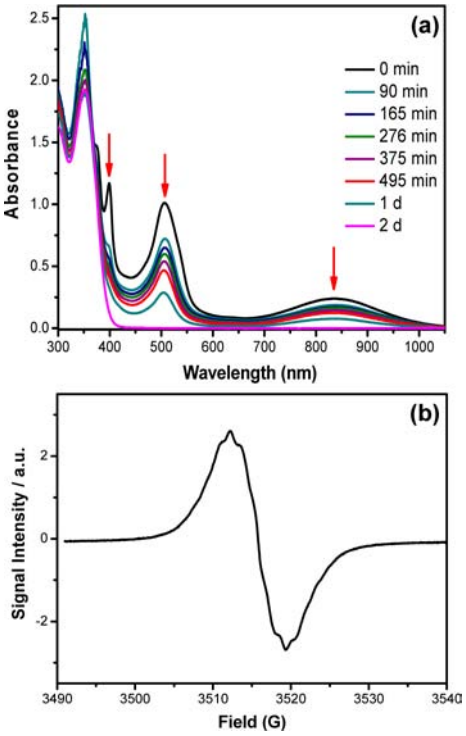

Figure 2. (a) Change of UV−vis absorption spectra of the freshly generated **1-OS** biradical with time. (b) ESR spectrum of **1-OS** in chloroform recorded at room temperature.

absorption spectrum is characteristic of typical open-shell PAHs with unpaired electrons. The existence of the biradical was further proved by the strong electron spin resonance (ESR) signal (g = 2.0029) showing unresolved hyperfine coupling, obtained for the fresh **1-OS** solution generated in chloroform (Figure 2b), indicating a paramagnetic character of the biradical at room temperature.

The time-dependent UV−vis−NIR absorption spectra of the newly generated biradical underwent a slow decay process (Figure 2a). That is, the absorption spectrum of the biradical **1-OS** slowly decreased with time (indicated by the arrow) and reached zero absorbance in 2 days (at the three major absorbances), and the final absorption spectrum after decay was identical to that of **1-CS**. This slow relaxation process was also followed by ^{1}H NMR measurements (Figure S1 in the Supporting Information), which clearly confirmed a transition from an unstable biradical form (**1-OS**) to a stable quinoidal form (**1-CS**). The plot of the absorbance ($\ln(A_t)$) at 834 nm of the freshly prepared **1-OS** in toluene with time revealed a monoexponential decay from the biradical **1-OS** to the quinoidal form **1-CS** at 298 K, with a half-life of around 495 min (Figure 3a). The decay reaction rate constant (k) under this condition was determined to be 0.0014 min^{-1}. To further determine the thermodynamic parameters for this decay process, same decay experiments were conducted at least three times at different temperatures in toluene, and thus the average decay reaction rate constants at respective temperature were obtained (Figure S2 in the Supporting Information). The

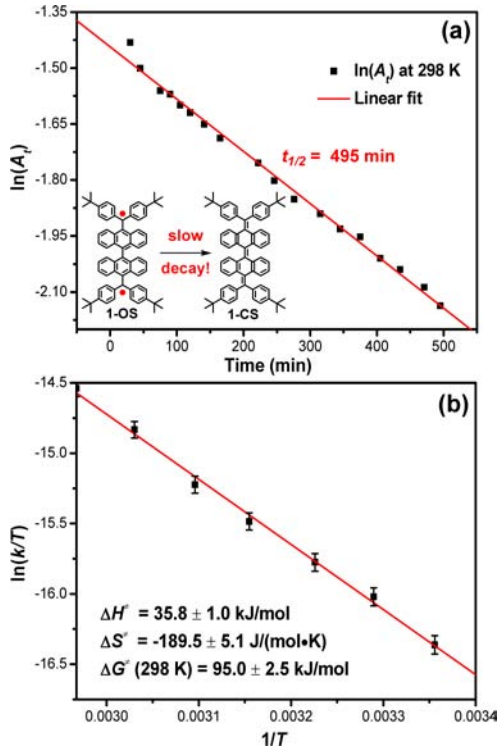

Figure 3. (a) Monoexponential decay of the absorbance at 834 nm of the freshly generated **1-OS** biradical with time at 298 K. R^2, 0.9934; standard error, 0.00786. (b) $\ln(k/T) \approx 1/T$ plot for the decay of **1-OS** at variable temperatures (298−337 K), based on thermodynamic data obtained by fitting the data with Eyring equation.

value of $\ln(k/T)$ was plotted with $1/T$, and a straight line was obtained (Figure 3b). The data were fit by the Eyring equation:

$$\ln\left(\frac{k}{T}\right) = -\frac{\Delta H^{\ddagger}}{R}\cdot\frac{1}{T} + \ln\left(\frac{k_B}{h}\right) + \frac{\Delta S^{\ddagger}}{R}$$

in which k is the reaction rate constant, T is the absolute temperature, $\Delta H^{\ddagger}$ is the enthalpy of activation, R is the gas constant, k_B is the Boltzmann constant, h is the Planck constant, and the $\Delta S^{\ddagger}$ is the entropy of activation. The thermodynamic parameters for such an unusual decay process then were obtained, with $\Delta H^{\ddagger}$ = 38.5 ± 5.1 kJ mol^{-1} and $\Delta S^{\ddagger}$ = −189.5 ± 0.6 J mol^{-1} K^{-1}. Accordingly, the Gibbs energy of activation $\Delta G^{\ddagger}$ ($\Delta H^{\ddagger} - T\Delta S^{\ddagger}$) was determined as 95.0 ± 2.5 kJ mol^{-1} at 298 K. The result means that such a transition from the biradical form to the quinoidal form requires overcoming a high energy barrier. The large negative $\Delta S^{\ddagger}$ value also indicates a conversion from a disordered structure to a highly ordered conformation (i.e., the highly contorted butterfly structure for **1-CS**).

DFT calculations (UCAM-B3LYP/6-31G*)[28] were then conducted to provide a further understanding of such an unusual decay process. The optimized geometries of the **1-CS** and **2-OS** are shown in Figure 4. Molecule **1-CS** also has a butterfly-like geometry with a typical quinoidal character, which is consistent with its single-crystal structure. For **1-OS**, it possibly exists as a singlet or a triplet biradical. In comparison to the quinoidal **1-CS**, both the singlet and the triplet **1-OS** show longer bond lengths for the exo methylene bonds and the bond between the two anthracene units (labeled with arrow), indicating a distinct open-shell character of **1-OS**. In addition, the biradical **1-OS** adopts an orthogonal geometry for the

dx.doi.org/10.1021/ja3050579 | J. Am. Chem. Soc. 2012, 134, 14513−14525

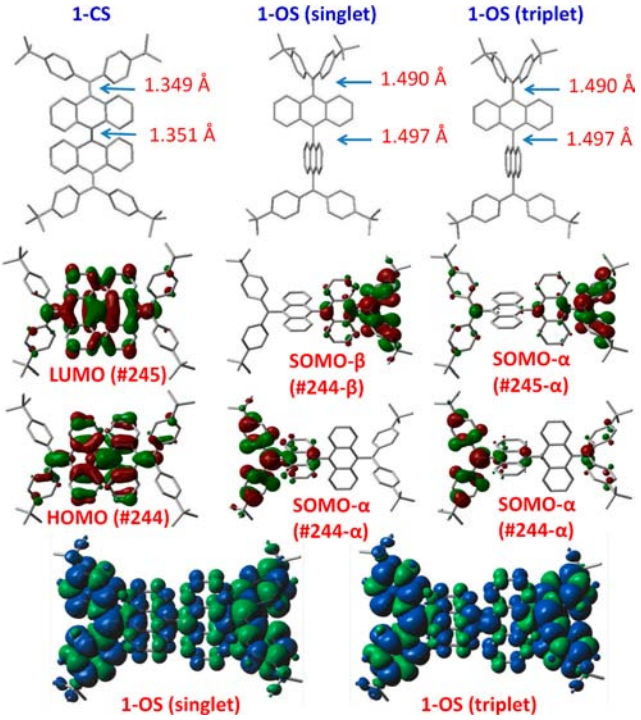

Figure 4. Calculated geometric structures (with part of the bonds labeled with length in Å) and the frontier molecular orbitals of the closed-shell **1-CS** and open-shell **1-OS** both in singlet and in triplet states. The bottom shows the spin density distribution of the singlet and triplet **1-OS**.

bisanthracene core with a dihedral angle of nearly 90°, indicating a transition from a quinoidal structure in **1-CS** to a benzenoid form in **1-OS**. This results in a large negative change of entropy from a disordered to an ordered conformer during the transition from **1-OS** to **1-CS**, which agrees well with the large negative $\Delta S^{\ddagger}$ value determined experimentally.

Calculations also revealed that the Gibbs energies of the singlet and triplet biradical form **1-OS** are located 18.4 and 15.9 kJ/mol higher than for the closed-shell **1-CS**, indicating that the quinoidal resonance form dominates the ground-state electronic and geometric structure and the **1-OS** can be regarded as a metastable excited state (see energy diagram in Figure 5). The

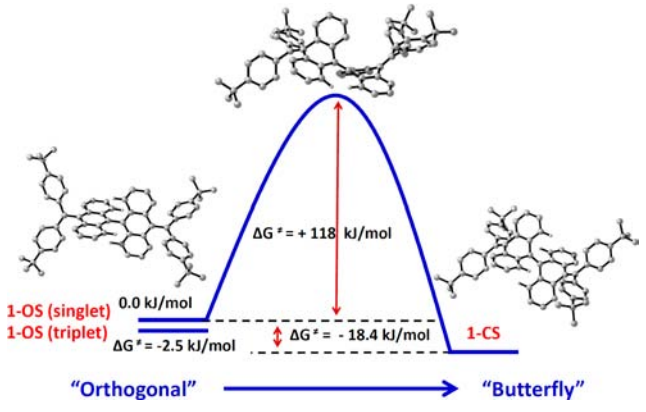

Figure 5. Calculated energy diagram for the **1-CS**, **1-OS** (singlet), and **1-OS** (triplet) and schematic representation of a transition from a higher-energy orthogonal biradical form to a lower-energy butterfly conformer through a high-energy transition state.

decay process mimics the monoexponential fluorescence decay of a chromophore from the excited state to the ground state. In addition, the energy level for the triplet **1-OS** is slightly lower (2.5 kJ/mol) than that of the singlet **1-OS**; thus the orthogonal biradical favors a triplet state, which is also consistent with the observed paramagnetic signal for the newly generated biradical **1-OS**. Upon conversion from the free-rotated orthogonal biradical to the lower-energy butterfly like quinoidal form, the molecule must overcome a high energy barrier to reach a transition state, in which the zigzag edges of the anthracene units are in close proximity with each other and with the four 4-*tert*-butylphenyl rings so that a conversion to a contorted butterfly conformation is possible (Figure 5). A considerable energy barrier of 118 kJ/mol was calculated, which is close to the experimental activation energy value (95 ± 2.5 kJ/mol) measured in solution at 298 K. It is worth noting that, in most cases, the conversion between different electronic configurations that are very close in energy in the ground electronic state occurs at very short time-scale and cannot be easily detected. However, in this case, because of a high activation energy needed for the intersystem crossing from **1-OS** to **1-CS**, an unusually slow decay process was observed experimentally.

1-CS displays the largest coefficients for the highest occupied molecular orbital (HOMO) and the lowest unoccupied molecular orbital (LUMO) along the quinoidal bisanthraquinodimethane moiety (Figure 4), indicating an extended π-electron delocalization despite its highly contorted structure. The two unpaired electrons (α and β spin) in the singlet **1-OS** show a disjointed singly occupied molecular orbital (SOMO), SOMO-α and SOMO-β, with orbital coefficients mainly localized at the terminal diphenylmethene units (Figure 4), indicating a large biradical character for **1-OS**. The spin-density distribution also presents a central symmetry with the terminal diphenylmethene units having the largest density, while there is still significant spin density distributed on the anthracene units (Figure 4). This suggested that the spins are delocalized, which can explain the good chemical stability of the intermediate biradical against oxidation and dimerization/oligomerization. The SOMO-α and SOMO-β profiles and the spin-distribution of the triplet **1-OS** indicate that the two spins are independent from each other, indicating a weak radical−radical coupling.

Synthesis and Characterizations of 2-CS/2-CS. To further tune the ground-state electronic and geometric structure of the tetrabenzo-Chichibabin's hydrocarbon, the two di(4-*tert*-butylphenyl)methene groups in **1-CS** were replaced by two fluorenyl units. The synthesis of **2-OS** was based on a similar synthetic concept as shown in Scheme 2. The 10,10′-dibromo-9,9′-bianthryl **6**[29] was treated with 2 equiv of *n*-BuLi followed by reaction with 9*H*-fluoren-9-one to give the precursor diol **7** in 65% yield. Subsequent reduction of **7** with $SnCl_2$ and purification of the crude product by routine column chromatography on silica gel afforded a deep red solid, which was identified as the biradical **2-OS**.

MALDI-TOF mass spectrum of this product agrees well with the molecular weight of compound **2-OS**. It is noteworthy that the absorption spectral patterns with vibronic splitting observed in the region of 300−400 nm are characteristic of that of anthracene.[30] In addition, a long absorption tail into the near-infrared region is attributed to the lowest energy transition with a small HOMO−LUMO energy gap of 1.28 eV. This steady-state optical property of **2-OS** suggests a representative open-shell biradical electronic structure as we expected (cf., Scheme 2). In this regard, this compound in THF-d_8 solvent did not

dx.doi.org/10.1021/ja3050579 | J. Am. Chem. Soc. 2012, 134, 14513−14525

Scheme 2. Synthetic Route of Compounds 2-OS and 2-CS[a]

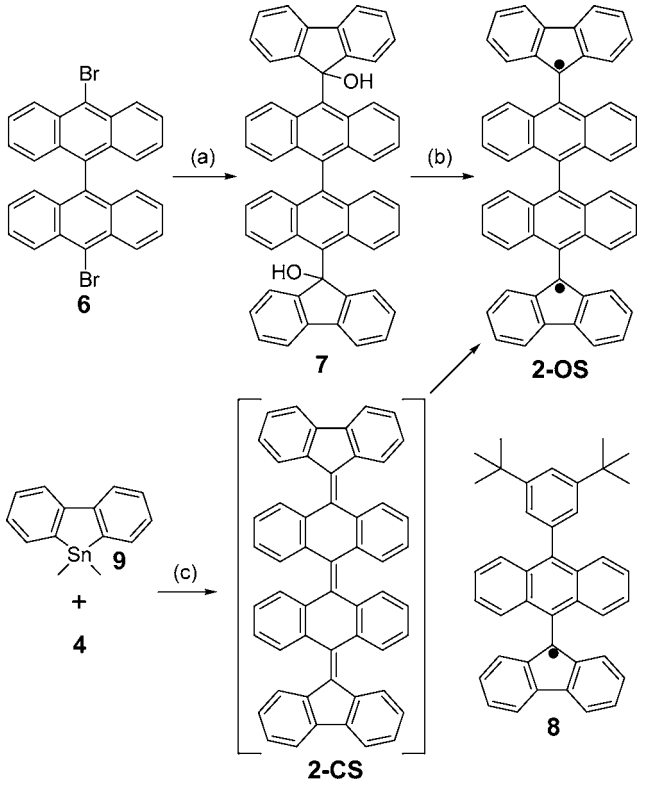

[a]Reaction conditions: (a) (1) *n*-BuLi/THF; (2) 9*H*-fluoren-9-one, 65%; (b) $SnCl_2$, CH_2Cl_2, room temperature, 82%; (c) $Pd(PBu^t_3)_4$, CuI, CsF, toluene.

show any NMR signals at room temperature even after cooling to −100 °C, indicating the presence of a considerable paramagnetic species. Strong ESR signal was detected for the sample in various solutions and in the solid state. For example, the solution of **2-OS** in 2-methyl tetrahydrofuran (2-Me−THF) showed a well-resolved quintet ESR spectrum with g = 2.0027 at 153 K (Figure 7a). Simulations indicated that most of the hyperfine structure resulted from two sets of two equivalent protons with hyperfine coupling constants of 4.1 and 3.2 G. Superconducting quantum interference device (SQUID) measurements were conducted for **2-OS** in the powder form at 5−380 K. The product of magnetic susceptibility χ and temperature T is plotted as a function of temperature in Figure 7b and the magnetic susceptibility can be well fitted with Bleaney−Bowers equation. The singlet−triplet gap was estimated to be $2J/k_B$ = 166 K (1.4 kJ/mol), indicating that the ground state for **2-OS** is triplet (paramagnetic). Thus, all of these experiments confirmed that the obtained compound was the biradical **2-OS** instead of the closed-shell form **2-CS**. Interestingly, **2-OS** displayed extremely high stability, and there was no obvious decomposition when the solution or solid was stored under ambient air and light conditions for months, which could be attributed to thermodynamic stabilization of the fluorenyl moieties and kinetic stabilization by the anthracene units.

To further understand the nature of the biradical in **2-OS**, an anthryl-substituted fluorenyl monoradical **8** (Scheme 2) was also prepared for comparison (see detailed synthesis in the Supporting Information). The UV−vis absorption spectrum (Figure 6) and the ESR spectrum (Figure 7) of compound **8**

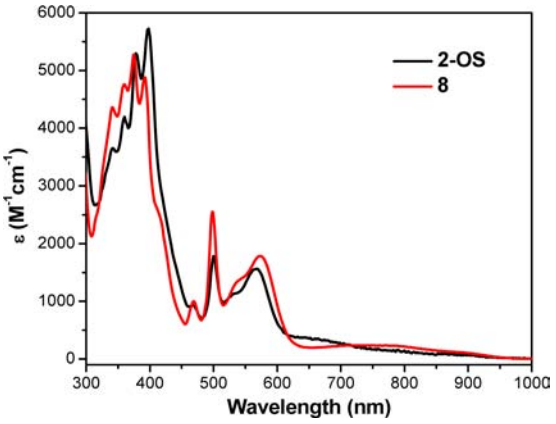

Figure 6. UV−vis−NIR absorption spectrum of **2-OS** and compound **8** in DCM.

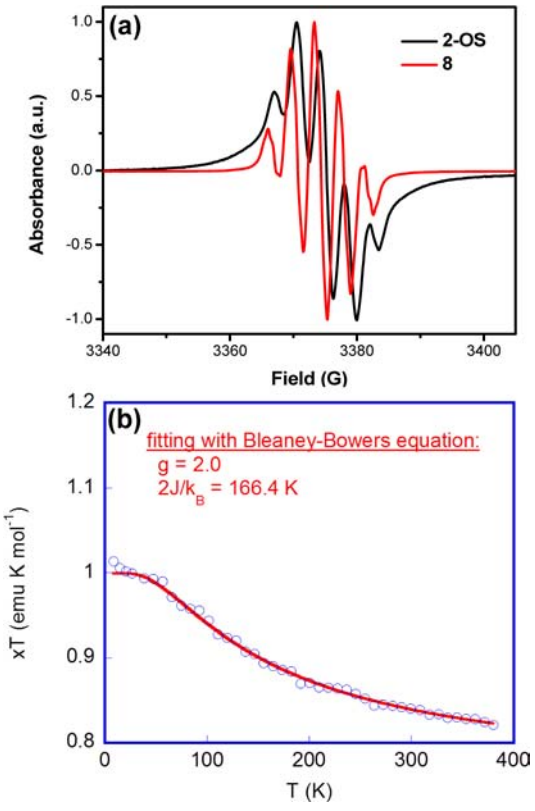

Figure 7. (a) CW ESR spectra of **2-OS** and **8** in 2-Me−THF at 153 K. (b) χT versus T curve for the powder of **2-OS** in the SQUID measurements and the fitting plot via the Bleaney−Bowers equation.

are very similar to that of **2-OS**, indicating that there is very weak dipole coupling between the two radicals. This is presumably due to the large mean internal radical-to-radical distance and the orthogonal arrangement of the two anthracene units in **2-OS** (vide infra). The small singlet−triplet energy gap (1.4 kJ/mol) obtained from the SQUID measurement also indicates a weak coupling between the two radicals, and both the singlet and triplet diradicals could exist at room temperature.

The existence of such a stable biradical character also implied that it may represent the ground-state structure of the **2-CS**/**2-OS**. To confirm this hypothesis, the synthesis of the closed-shell structure **2-CS** was also attempted (Scheme 2). This was

dx.doi.org/10.1021/ja3050579 | J. Am. Chem. Soc. 2012, 134, 14513−14525

done by the Still coupling reaction between compound **4** and 9,9-dimethyl-9-stannafluorene **9**[31] in the presence of Pd-$(PBu^t_3)_4$ as catalyst. However, the biradical form **2-OS** was generated instead of the closed-shell **2-CS**. This suggested that the closed-shell form **2-CS** was formed as an unstable intermediate compound, which quickly underwent relaxation to its more stable open-shell biradical form **2-OS**. The product **2-OS** could not be separated in its pure form by this method due to the contamination with other side-products including a ring-opening oligomer of **9**, which was identified by X-ray single-crystal analysis (Figure S3 in the Supporting Information). However, the formation of **2-OS** can be unambiguously identified by MALDI-TOF mass spectrum and UV−vis absorption measurement, which are identical to those for pure **2-OS**. Therefore, the ground state of **2-CS**/**2-OS** can be defined as the open-shelled biradical, which is in contrast to the **1-CS**/**1-OS** pair.

Similar theoretical calculations were also conducted for **2-CS**/**2-OS** (Figure 8). The closed-shell form of **2-CS** adopted a

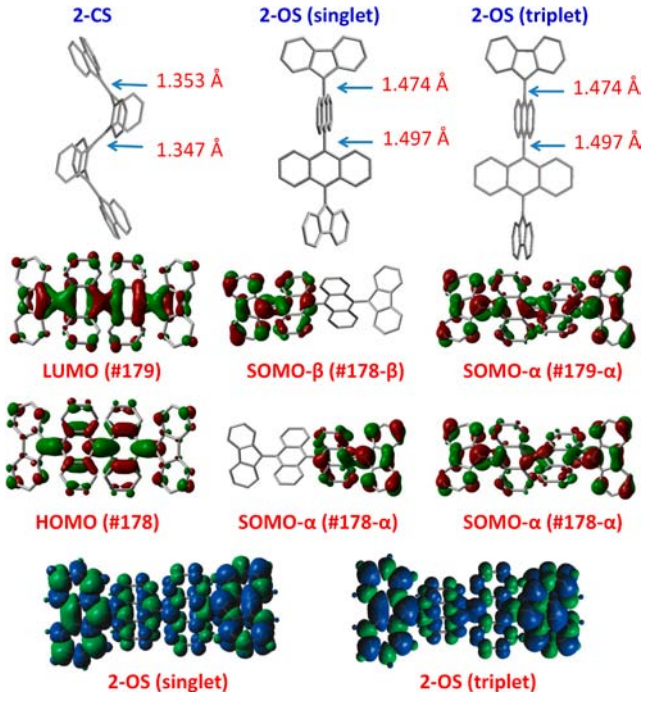

Figure 8. Calculated geometric structures (with part of the bonds labeled with length in Å) and the frontier molecular orbitals of the closed-shell **2-CS** and open-shell **2-OS** both in singlet and in triplet states. The bottom shows the spin density distribution of the singlet and triplet **2-OS**.

contorted butterfly conformation with characteristic bond lengths (as labeled with arrows, 1.353, 1.347 Å, respectively) for a quinoidal hydrocarbon, similar to **1-CS**. The open-shell **2-OS** structures show an orthogonal geometry due to steric congestion, similar to those for **1-OS** as well. DFT calculations showed that the diradical states (singlet and triplet **2-OS**) had lower energies than its closed-shell form (**2-CS**) by 23.4−25.9 kJ/mol, and the energy of the triplet state was slightly lower energy than the singlet biradical state by 2.5 kJ/mol, which is consistent with the SQUID measurement (ΔE_{S-T} = −1.4 kJ/mol). The frontier molecular orbital profiles of **2-CS** revealed that the electrons are mainly delocalized through the π-extended quinodimethane part at the middle of the molecule for both HOMO and LUMO. In contrast to **2-CS**, the SOMOs of the α and β spins in **2-OS** exhibit an extended delocalization to the fluorenyl unit, especially for the singlet state. Thus, **2-OS** showed large spin density at the fluorenyl moiety (Figure 8). The large spin delocalization through the fluorenyl anthryl methene unit should account for the high stability of the biradical.

Electrochemical Properties of 1-CS/2-OS and Their Dication 1-CS^{2+}/2-OS^{2+}. Cyclic voltammetry was performed to investigate electrochemical properties of **1-CS** and **2-OS**. **1-CS** in DCM exhibited one chemically irreversible reductive wave with half-wave potential E_{red} at −1.27 V (vs Fc^+/Fc), and the first oxidative scan revealed an intense irreversible oxidation wave above 0.73 V (Figure 9a). However, the reverse scan from the high oxidation state back to −0.6 V showed two closely overlapped quasi-reversible reduction waves. The second and third circle scans showed that the same redox waves existed. This observation suggested that subsequent chemical reaction

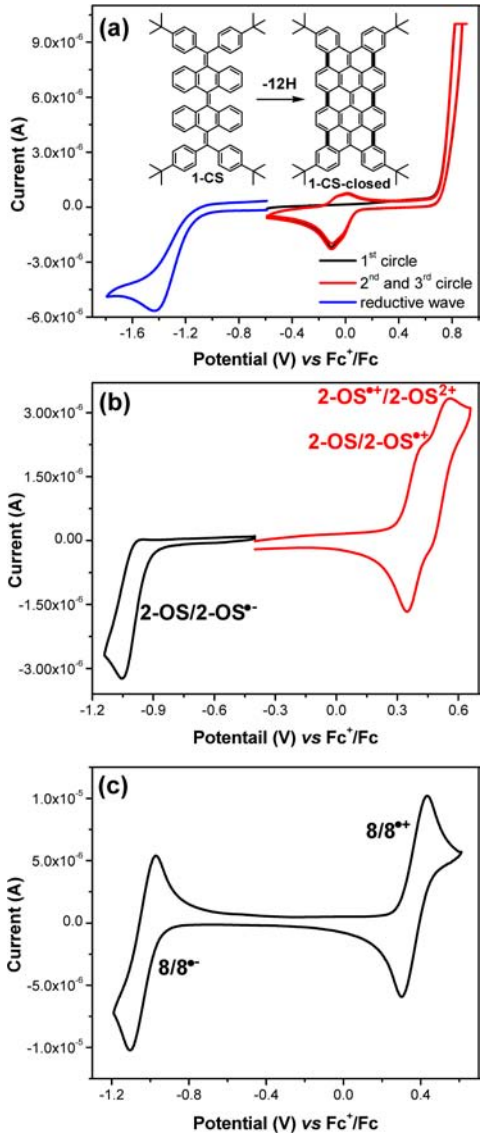

Figure 9. Cyclic voltammograms of **1-CS** (a), **2-OS** (b), and compound **8** (c) in dry DCM with 0.1 M Bu_4NPF_6 as supporting electrolyte, Ag/AgCl as reference electrode, Au disk as working electrode, Pt wire as counter electrode, and a scan rate at 100 mV/s.

dx.doi.org/10.1021/ja3050579 | J. Am. Chem. Soc. 2012, 134, 14513−14525

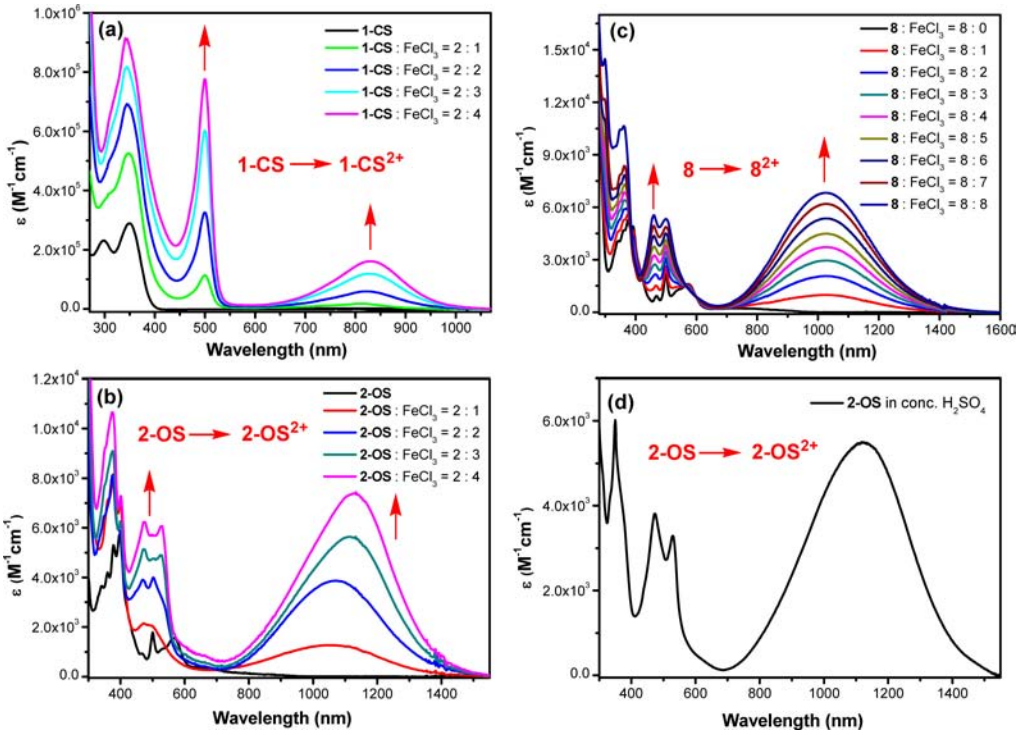

Figure 10. UV−vis−NIR absorption spectra of **1-CS** (a), **2-OS** (b), and compound **8** (c) upon oxidative titration with $FeCl_3$ in dry DCM, and absorption spectrum of **2-OS** in concentrated H_2SO_4 (d).

might happen after the oxidation of **1-CS** at high potential (>0.73 V) so that a new redox active species with lower oxidation potential was generated. Electrolysis of the **1-CS** in DCM was then conducted at 1.0 V using a large Pt plate electrode, and the mixture was monitored by MALDI-TOF mass spectroscopy. Interestingly, the mass spectrum of the mixture revealed the existence of the starting material and a species with a loss of 12 hydrogen atoms (Figure S4 in the Supporting Information). Thus, an intramolecular oxidative cyclodehydrogenation likely occurred at the high oxidation potentials, which gave the fully fused hydrocarbon **1-CS-closed** (inserted structure shown in Figure 9a) via the loss of 12 hydrogen atoms.[32] Compound **2-OS** exhibited two reversible oxidation waves with half-wave potentials E_{ox}^1 = 0.38 V and E_{ox}^2 = 0.52 V (vs Fc^+/Fc), and one quasi-reversible reduction wave with a half-wave potential E_{red} = −0.98 (vs Fc^+/Fc) (Figure 9b). The energy levels of the HOMO and LUMO were determined to be −5.10 and −3.87 eV, respectively, from the onset potentials of the oxidation and reduction waves. Thus, a low electrochemical energy gap (E_g^{EC}) of 1.23 eV was determined for **2-OS**, which was consistent with its optical energy gaps (E_g^{Opt} = 1.28 eV). Such a small energy gap promoted **2-OS** to adopt open-shell biradical in the ground state. These two oxidative waves suggest that compound **2-OS** can be oxidized to its monoradical cation and dication after removal of one and two unpaired electrons. For comparison, the monoradical **8** showed one reversible oxidation wave at E_{ox} = 0.37 V and one reversible reduction wave at E_{red} = −1.04 V (Figure 9c), with the HOMO and LUMO energy levels being −5.10 and −3.84 eV, respectively.

The low oxidation potentials observed for **1-CS** and **2-OS** allowed us to approach their cationic species (monoradical cation and dication) by chemical oxidation. Instead of using highly reactive and expensive oxidants such as super acid SbF_5/SO_2ClF, which are usually used for generating aromatic or antiaromatic carbocations of hydrocarbons at very low temperature.[33] We found that mild oxidants such as $FeCl_3$ could be used for the oxidation of **1-CS**/**2-OS** into their corresponding dications in nearly quantitative yield at room temperature. Chemical oxidative titration of compounds **1-CS** and **2-OS** by $FeCl_3$ was conducted in dry DCM, and the progress was monitored by UV−vis−NIR spectroscopy (Figure 10a and b). Both compounds can be oxidized by $FeCl_3$ into stable cationic species, and the absorbance reached a saturation state when 2 equiv of $FeCl_3$ was used, indicating formation of stable dications. This is consistent with the previous observation that attempted cyclodehydrogenation of **1-CS** with $FeCl_3$ followed by quenching with aqueous solution gave the diol **5**. A new sharp and intense absorption band at 500 nm and a broad absorption band centered at 832 nm were observed for the dication **1-CS**$^{2+}$. Similarly, for **2-OS**, titration with $FeCl_3$ finally led to a well-resolved band with maximum at 528 and 475 nm, and a new broad band with maximum at 1130 nm for the dication **2-OS**$^{2+}$. It should be noted that in both cases, the broad bands were bathochromically shifted obviously during the titration before reaching the final state, indicating the existence of both monoradical cation and dication at the intermediate stage. Under the same condition, compound **8** can be progressively oxidized by $FeCl_3$ into its monocation (Figure 10c), and a broad band centered at 1027 nm together with a well-resolved band at 500/458 nm were observed. The band structure was similar to that for **2-OS**$^{2+}$ due to their similar chemical structure.

Although the preparation of the parent 9-fluorenyl cation in sulfuric acid was difficult due to rapid decomposition and polymerization to unidentifiable products,[34] we found that the oxidation of **2-OS** in concentrated sulfuric acid gave a stable dication **2-OS**$^{2+}$, which permitted UV−vis−NIR absorption and

dx.doi.org/10.1021/ja3050579 | J. Am. Chem. Soc. 2012, 134, 14513−14525

^{1}H NMR spectroscopic measurements. As shown in Figure 10d, the UV−vis−NIR spectrum of compound **2-OS** in concentrated H_2SO_4 is nearly identical to the dication **2-OS**$^{2+}$ generated from oxidation of **2-OS** with $FeCl_3$, indicating that the dication species was indeed formed upon mixing **2-OS** with concentrated H_2SO_4. The ^{1}H NMR spectrum of **2-OS**$^{2+}$ was then recorded in D_2SO_4, and well-resolved aromatic proton resonances appeared after 2 h, which could be clearly assigned to the desired dication **2-OS**$^{2+}$ (Figure S5). It was worthy to note that the protons on the fluorenyl unit showed obvious shift to the high field, indicating an antiaromatic nature of the cyclopentadienyl cation. The dication solution in sulfuric acid was quite stable and showed no change after storage at room temperature for several weeks. However, oxidation of the **1-CS** and compound **8** with concentrated H_2SO_4 led to a complicated mixture due to decomposition of the starting materials.

Subsequently, DFT (UCAM-B3LYP) calculations were conducted to further understand the stability of the dications **1-CS**$^{2+}$ and **2-OS**$^{2+}$. In both cases, high HOMO coeficients are mainly found at the anthracene units, while the LUMO coeficients are mainly localized at the diphenylmethane or fluorenyl moieties (Figure 11). The Mulliken charge density

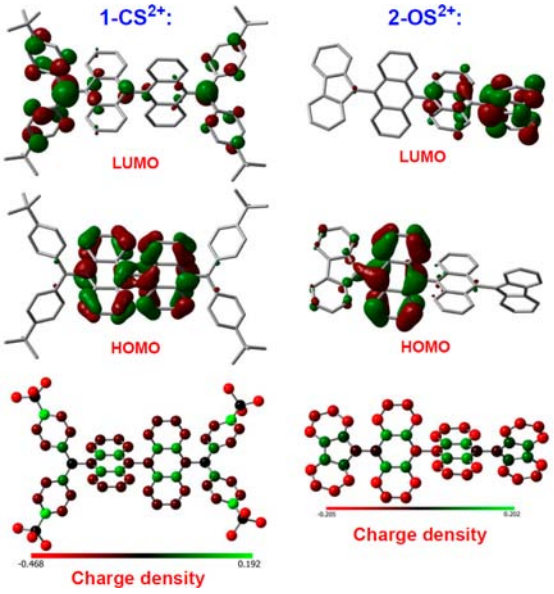

Figure 11. Calculated frontier molecular orbital profiles and the Mulliken charge density distribution of **1-CS**$^{2+}$ and **2-OS**$^{2+}$.

distribution indicated that the positive charges are mainly localized at the methane cation site but also delocalized through the anthracene units and the diphenyl or fluorenyl moieties. Such a charge delocalization should account for the good stability of the dications **1-CS**$^{2+}$ and **2-OS**$^{2+}$.

FT Raman Spectra of 1-CS/2-OS and Their Dications. To scrutinize the intrinsic structure of **1-CS**/**2-OS** in neutral state and their corresponding dications **1-CS**$^{2+}$/**2-OS**$^{2+}$, FT Raman experiments were conducted and provided further structure−property relationships between the closed-shell and open-shell species.[35] FT-Raman spectra of **1-CS** and **2-OS** in their neutral states are shown in Figure 12, and there is a large difference between the two spectra in the 1600 cm^{-1} region. The spectrum of **1-CS** has clear signatures of benzo-quinoidal rings (i.e., band at 1596 cm^{-1}) together with a band at a

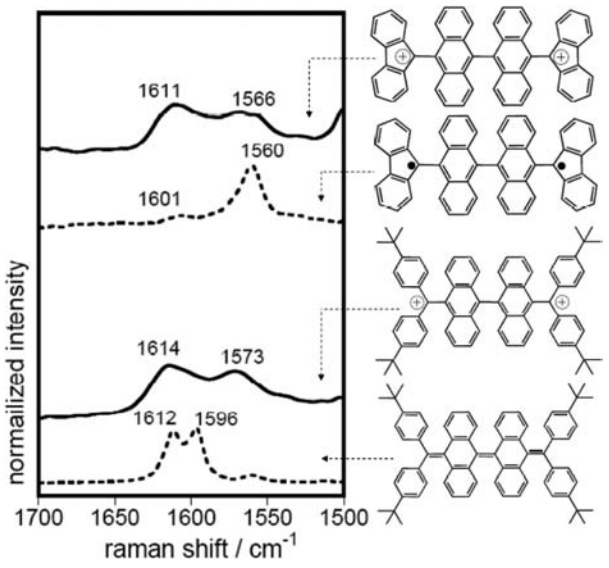

Figure 12. 1064 nm FT-Raman spectra of neutral and oxidized **1-CS** (bottom: dotted and solid lines, respectively) and of neutral and oxidized **2-OS** (top: dotted and solid lines, respectively).

position close to that of usual conjugated C═C bond stretches (i.e., band at 1612 cm^{-1}), which indicates that the structure of **1-CS** is compatible with a closed-shell electronic configuration. The spectrum of **2-OS**, however, with the strongest band at 1560 cm^{-1}, reveals its anthracene-like structure originated from the stabilization of the open-shell aromatized species. The evolution from a closed-shell structure in **1-CS** to an open-shell structure in **2-OS** as delineated by the Raman spectra can be interpreted by the larger stabilization energy of the radical center in a planar cyclopentadienyl moiety in **2-OS**, a structural motif that is not possible in **1-CS**.

The unique absorbance tail of **2-OS** from 500 nm to the near-infrared (Figure 6), likely due to the open-shell structure, allows us to use resonance Raman spectroscopy to get further insights onto the electronic configuration by comparing the Raman spectra of **2-OS** recorded with the 633 and 1064 nm excitation wavelengths, which correspond to on-resonance and off-resonance experiments, respectively (Figure S6 in the Supporting Information). The spectra of **2-OS** under different excitation wavelengths are essentially identical, highlighting that there is a sole electronic configuration describing the ground electronic state. On the other hand, the VT FT-Raman spectra for **1-CS** and **2-OS** in the solid state (Figure S7 in the Supporting Information) showed that between −170 and +120 °C the Raman spectra are almost unaltered, revealing the absence of any relevant thermal interpopulation between low energy lying states; that is, **1-CS** and **2-OS** are robust singlet and triplet ground electronic states, respectively. For **2-OS**, the thermal invariance of the Raman spectra might indicate almost iso-energetic singlet and triplet states or a rather small singlet−triplet energy gap, which is in accordance with both theoretical calculations and experimental measurements.

These two samples were oxidized to their corresponding dications by $FeCl_3$ in dry DCM, and the FT-Raman spectra of the oxidized species in solution are also shown in Figure 12. These two spectra correspond to resonance Raman spectra as the 1064 nm laser of the Raman experiment excites the characteristic electronic absorptions of both dicationic species (Figure 10). This is important because it discards interference

dx.doi.org/10.1021/ja3050579 | J. Am. Chem. Soc. 2012, 134, 14513−14525

by other species. Conversely to the case of the neutral systems, the two spectra now became similar (Figure 12), suggesting that both species shared a similar geometrical structure in their charged ground electronic states. The appearance of the intense band in the two oxidized species around 1570 cm^{-1} can be assigned to the anthracene-like structure of the two molecular cores, which was in accordance with the formation of the corresponding carbocations either in the fluorenyl center in **2-OS** or in the diphenylmethene center in **1-CS**. Thus, our Raman spectroscopic measurements clearly revealed the ground-state electronic structures of **1-CS**/**2-OS** and their dications, which were consistent with the previous studies by other approaches.

Femtosecond Transient Absorption and Two-Photon Absorption Spectroscopic Measurements. To date, the excited-state dynamics of open-shell organic molecules has been still rarely investigated because of the limited number of systems with stable radical-associated molecules suitable for testing these effects. A few hybrid derivatives possessing the stable heteroatomic spin center on N−O units (e.g., TEMPO and α-nitronylnitroxide) have been characterized by transient absorption spectroscopy.[36] In contrast to the spin-localized heteroatomic systems, the spin-delocalized pure PAHs would exhibit the different relaxation nature in their excited states. The effect of open-shell electronic structure of **2-OS** on the excited-state photophysical properties is of interest. Therefore, we carried out the femtosecond transient absorption (TA) measurements to investigate the excited-state dynamics of **1-CS** and **2-OS** (Figures S8,S9 in the Supporting Information). For compound **1-CS** in toluene at room temperature, the broad excited-state absorption (ESA) signals around 700 nm become narrower and hypsochromically shifted to 670 nm within an initial 15 ps time decay, probably due to the conformational change through the internal conversion process from the higher excited state. The two decay-associated spectra at early time-evolution and the longer one indicate the TA spectra before and after vibrational relaxation process, respectively. The decay time constants probed at various wavelengths are fitted by two exponential functions of 7 and 96 ps. The singlet excited-state lifetime of **1-CS** estimated to be 96 ps is relatively shorter presumably due to the structural flexibility resulting from the contorted butterfly geometry.

In the case of **2-OS**, the broad ESA signal was observed in the whole visible region. The decay profile probed at 736 nm was estimated to be 24 ps by fitting with a single exponential function. As compared to the closed-shell **1-CS**, the open-shell derivative **2-OS** had a more short-lived excited-state lifetime. While the structure-dependent radical-induced quenching mechanism[36b] through enhanced intersystem crossing (ISC) and/or internal conversion (IC) in doublet radical−chromophore dyads has been reported, the fast decay kinetic profile of **2-OS** is considered to reflect an acceleration of the nonradiative IC rates arising from the smaller energy gap between the lowest excited state and the open-shell ground state. The non-fluorescent property of **2-OS** is also consistent with the short excited-state lifetimes. Considering the relatively rigid orthogonal structure of **2-OS** containing aromatized anthracene units, the unpaired electrons associated with the molecule contributed to the ultrafast relaxation dynamics.

To investigate the NLO properties of the biradical **2-OS**, two-photon absorption measurements were conducted by using the open-aperture Z-scan method with 130 fs pulses in the NIR region from 1200 to 1500 nm where one-photon absorption (OPA) contribution is negligible. As shown in Figure 13 (and Figure S10 in the Supporting Information), although **2-OS** had

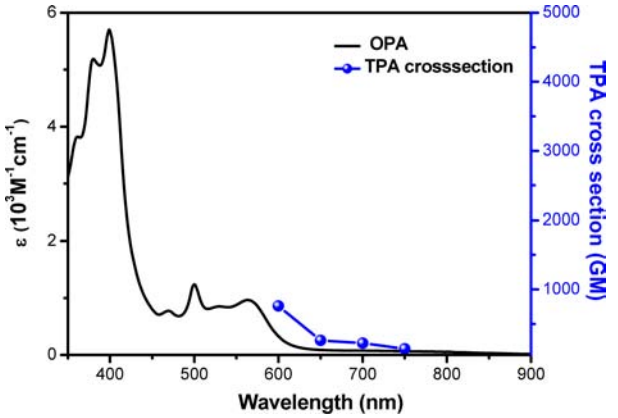

Figure 13. OPA (black solid line and left vertical axis) and TPA spectra (blue symbols and right vertical axis) of **2-OS** in chloroform. TPA spectra were plotted at $\lambda_{ex}/2$.

a rather small OPA absorption coefficient, it showed a large TPA cross section in the wavelength region with the maximum value as 760 GM at 1200 nm. In comparison with typical hydrocarbon chromophores, which only exhibited a small TPA value at the long wavelength, a relatively larger cross section for compound **2-OS** was obtained, and was comparable to the achieved value of other open-shell PAH molecules (300−890 GM)[4] in the same region of photoexcitation. This result can be reasonably understood by the unusual ground-state electronic structure of **2-OS** with distinct biradical character. The measurement on the closed-shell **1-CS** however was limited by its too short absorption wavelength, which was out of the range of the photoexcitation wavelength of our facilities.

III. CONCLUSION

In summary, two new stable tetrabenzo-Chichibabin's hydrocarbons were synthesized by a new strategy, and their electronic structure and geometry in the ground state were investigated by various experiments assisted by DFT calculations. Their ground-state structures were tunable, with **1-CS** as a closed-shell hydrocarbon and **2-OS** as an open-shell biradical. Such a difference can be explained by an enhanced thermodynamic stabilization of the biradicaloid resonance form when the di(4-*tert*-butylphenyl)methene groups in **1-CS** were replaced by fluorenyl units in **2-OS**. The extremely high stability of the biradical **2-OS** can be ascribed to thermodynamic stabilization by delocalization and kinetic blocking by the anthracene units. Their excited states were also approachable by chemical means, and an unusually slow transition from the orthogonal **1-OS** to a highly contorted butterfly like **1-CS** was observed, which can be explained by a very large energy barrier arising from steric repulsion during the transition. A quinoidal form **2-CS** represented the excited state of **2-OS**, and it quickly relaxed back to the ground state during chemical synthesis. The nature of the biradical in **2-OS** was confirmed as two weakly coupled radicals with a triplet ground state and a small singlet−triplet energy gap (ΔE_{S-T} = −1.4 kJ/mol). Both compounds can be oxidized into stable dications by chemical oxidation. FT Raman spectroscopy also provided further structural information, such as a quinoidal form for **1-CS** and a benzenoid form for **2-OS**, **1-CS**$^{2+}$, and **2-OS**$^{2+}$, which was consistent with other

dx.doi.org/10.1021/ja3050579 | J. Am. Chem. Soc. 2012, 134, 14513−14525

experimental data. The open-shell **2-OS** has a shorter singlet excited lifetime than that of closed-shell **1-OS**, which can be considered to reflect a radical-induced acceleration of the nonradiative internal conversion rates. Moreover, the open-shell **2-OS** exhibited a large TPA cross-section value (760 GM) at long wavelength (1200 nm), indicating promising potential applications of open-shell PAHs in nonlinear optics.

IV. EXPERIMENTAL SECTION

Steady-state UV−vis absorption and fluorescence spectra were recorded on a Shimadzu UV-1700 spectrometer and a RF-5301 fluorometer, respectively. The electrochemical measurements were carried out in anhydrous DCM with 0.1 M Bu_4NPF_6 as the supporting electrolyte at a scan rate of 100 mV/s at room temperature under the protection of nitrogen. A gold disk was used as working electrode, platinum wire was used as counting electrode, and Ag/AgCl (3 M KCl solution) was used as reference electrode. The potential was externally calibrated against the ferrocene/ferrocenium couple. Continuous wave X-band ESR spectra were obtained with a Bruker ELEXSYS E500 spectrometer using a variable-temperature Bruker liquid nitrogen cryostat. Quantitative ESR experiments were conducted by over-modulating the EPR signals and comparing the signal intensities of **8** and **2-OS** with the long-lived radical anion produced by the one-electron reduction of vitamin K1[37] obtained under identical instrumental and experimental conditions. The integrated ESR signals of 1 mM solutions of each radical were obtained separately in a silica flat cell. The observation that compounds **8** show integrated signal intensities similar to that of $VK1^{\bullet-}$ confirms that they are the primary radicals, and the signal is not due to minor impurities. The signal intensity of **2-OS** is 1.77 times that of **8**, indicating the existence of diradicals containing both singlet and triplet species. A SQUID system (Quantum Design, 5T) was used for the magnetic characterization in the temperature range of 5−380 K. The powder of **2-OS** powder (9 mg) was sealed in a plastic tube. Magnetic susceptibility was measured under a constant magnetic field of 3000 Oe in the temperature range of 5−380 K. The signal of sample holder and plastic tube was deducted by measuring the sample holder and plastic tube under same conditions. For the analysis of the raw SQUID data, we assumed that the magnetic susceptibility of the **2-OS** sample consists of three components, diamagnetic signal, paramagnetic impurity, and signal of singlet−triplet (which can be described with the Bleaney−Bowers equation).

FT−Raman spectra were measured using an FT-Raman accessory kit (FRA/106-S) of a Bruker Equinox 55 FT-IR interferometer. A continuous-wave Nd-YAG laser working at 1064 nm was employed for excitation, at a laser power in the sample not exceeding 30 mW. A germanium detector operating at liquid nitrogen temperature was used. Raman scattering radiation was collected in a back-scattering configuration with a standard spectral resolution of 4 cm^{-1}. 2000 scans were averaged for each spectrum. A variable-temperature cell Specac P/N 21525, with interchangeable pairs of quartz windows, was used to record the FT-Raman spectra at different temperatures. The variable-temperature cell consists of a surrounding vacuum jacket (0.5 Torr) and combines a refrigerant Dewar and a heating block as the sample holder. It is also equipped with a copper constantan thermocouple for temperature monitoring between −170 and 150 °C. Samples were inserted into the heating block part or the Dewar/cell holder assembly in the form of pure solids dispersed in KBr pellets, and Raman spectra were recorded after waiting for thermal equilibrium in the sample. The samples in KBr pellets were prepared in an oxygen- and water-free bag.

The femtosecond time-resolved transient absorption spectrometer used for this study consisted of a femtosecond optical parametric amplifier (Quantronix, Palitra-FS) pumped by a Ti:sapphire regenerative amplifier system (Quantronix, Integra-C) operating at 1 kHz repetition rate and an accompanying optical detection system. The generated OPA pulses had a pulse width of ∼100 fs and an average power of 1 mW in the range 450−800 nm, which were used as pump pulses. White light continuum (WLC) probe pulses were generated using a sapphire window (2 mm thick) by focusing of small portion of the fundamental 800 nm pulses, which were picked off by a quartz plate before entering into the OPA. The time delay between pump and probe beams was carefully controlled by making the pump beam travel along a variable optical delay (Newport, ILS250). Intensities of the spectrally dispersed WLC probe pulses were monitored by miniature spectrograph (OceanOptics, USB2000+). To obtain the time-resolved transient absorption difference signal (ΔA) at a specific time, the pump pulses were chopped at 25 Hz, and absorption spectra intensities were saved alternately with or without pump pulse. Typically, 6000 pulses were used excite samples and to obtain the TA spectra at a particular delay time. The polarization angle between pump and probe beam was set at the magic angle (54.7°) using a Glan-laser polarizer with a half-wave retarder to prevent polarization-dependent signals. The cross-correlation fwhm in the pump−probe experiments was less than 200 fs, and chirp of WLC probe pulses was measured to be 800 fs in the 400−800 nm regions. To minimize chirp, all reflection optics were used in the probe beam path, and a quartz cell of 2 mm path length was employed. After each set of fluorescence and TA experiments was completed, the absorption spectra of all compounds were carefully checked to rule out the presence of artifacts or spurious signals arising from, for example, degradation or photo-oxidation of the samples in question.

The two-photon absorption spectrum was measured in the NIR region using the open-aperture Z-scan method with 130 fs pulses from an optical parametric amplifier (Light Conversion, TOPAS) operating at a repetition rate of 3 kHz generated from a Ti:sapphire regenerative amplifier system (Spectra-Physics, Hurricane). After passing through a 10 cm focal length lens, the laser beam was focused and passed through a 1 mm quartz cell. Because the position of the sample cell could be controlled along the laser beam direction (z axis) using the motorcontrolled delay stage, the local power density within the sample cell could be simply controlled under constant laser intensity. The transmitted laser beam from the sample cell was then detected by the same photodiode as used for reference monitoring. The on-axis peak intensity of the incident pulses at the focal point, I_0, ranged from 40 to 60 GW cm^{-2}. For a Gaussian beam profile, the nonlinear absorption coefficient can be obtained by curve fitting of the observed open-aperture traces $T(z)$ with the following equation:

$$T(z) = 1 - \frac{\beta I_0 (1 - e^{-\alpha_0 l})}{2\alpha_0 [1 + (z/z_0)^2]}$$

where α_0 is the linear absorption coefficient, l is the sample length, and z_0 is the diffraction length of the incident beam. After the nonlinear absorption coefficient has been obtained, the TPA cross section $\sigma^{(2)}$ of one solute molecule (in units of GM, where 1 GM = 10^{-50} cm^4 s $photon^{-1}$ $molecule^{-1}$) can be determined by using the following relationship:

$$\beta = \frac{10^{-3}\sigma^{(2)} N_A d}{h\nu}$$

where N_A is the Avogadro constant, d is the concentration of the compound in solution, h is the Planck constant, and ν is the frequency of the incident laser beam.

Theoretical calculations were carried out by using the Gaussian 09 program. The initial geometry optimizations of **1-CS**/**1-OS** and **2-CS**/**2-OS** were performed with the UCAM-B3LYP/6-31G* level of theory.[28,38] The resulting DFT solution (i.e., singlet "closed-shell": zero spin density on all atoms) was further tested for its stability with the STABLE=OPT keyword. A spin symmetry broken DFT solution was found with lower energy for **2-OS**. Next, the Guess=Read keyword was used to perform the optimization at the same level. Frequency calculations were conducted to ensure that these structures are indeed local minima (see the Supporting Information for a summary of the computation results).

Synthesis of Tetrabenzo-Chichibabin's Hydrocarbon 1-CS. A mixture of **4** (500 mg, 0.72 mmol), 4-*tert*-butylphenylboronic acid (1.302 g, 7.23 mmol), K_2CO_3 (1.0 g, 7.23 mmol), Cs_2CO_3 (940 mg, 2.89 mmol), and $Pd(PPh_3)_4$ (330 mg, 0.029 mmol) in the mixed solvents of toluene (100 mL), ethanol (1 mL), and water (3.6 mL)

dx.doi.org/10.1021/ja3050579 | J. Am. Chem. Soc. 2012, 134, 14513−14525

was degassed and purged with argon three times. The mixture was heated to 130 °C for 48 h. After being cooled, the reaction mixture was concentrated in vacuum and then diluted with DCM (200 mL), and washed with water (100 mL) and brine (100 mL). The combined organic extracts were dried over anhydrous Na_2SO_4 and filtered, and the solvent was removed in vacuo. The residue was then purified by column chromatography (silica gel, DCM/hexane = 1:10) to afford the desired product (600 mg, 90%) as a white solid. ^{1}H NMR ($CDCl_3$, 500 MHz): δ ppm 7.41 (d, J = 8.5 Hz, 8H, Ar), 7.32 (d, J = 8.5 Hz, 8H, Ar), 7.15 (d, J = 7.5 Hz, 4H, Ar), 7.08 (d, J = 7.5 Hz, 4H, Ar), 6.87 (t, 4H, J = 7.0 Hz, Ar), 6.82 (t, 4H, J = 7.0 Hz, Ar), 1.32 (s, 36H, CH_3). ^{13}C NMR ($CDCl_3$, 75 MHz): δ ppm 149.41, 139.98, 139.64, 138.89, 137.59, 135.07, 132.14, 129.28, 128.64, 128.24, 125.46, 125.08, 124.74, 34.47, 31.38. High-resolution mass spectrum (HR MS) (EI): caldc for $C_{70}H_{68}$, 908.5321; found, m/z = 908.5329 (error = +0.9 ppm).

Synthesis of Tetrabenzo-Chichibabin's Hydrocarbon 2-OS. Under a nitrogen atmosphere, a solution of **7** (105 mg, 0.147 mmol) in dry DCM (30 mL) was added to $SnCl_2$ (139 mg, 0.735 mmol). The mixture was stirred overnight at room temperature under a nitrogen atmosphere. The solvent was removed under reduced pressure. The residue was then purified by column chromatography (silica gel, chloroform/hexane = 1:20) to give compound **2-OS** as a red solid (82 mg, 82%). HR MS (APCI): calcd for $C_{54}H_{32}$, 680.2504; found, m/z = 680.2506 (error = +0.3 ppm). No NMR signal was observed at room temperature even at low temperature (−100 °C). The purity was further determined by HPLC analysis with a silica column by using different eluents. Under variable conditions, only one elution peak was observed, indicating high purity of this compound (Figure S10 in the Supporting Information).

■ ASSOCIATED CONTENT

Supporting Information

Synthetic procedures and characterization data of all other new compounds. TA spectra and Z-scan curves. Crystallographic data. This material is available free of charge via the Internet at http://pubs.acs.org.

■ AUTHOR INFORMATION

Corresponding Author

chmwuj@nus.edu.sg; dongho@yonsei.ac.kr; kuowei.huang@kaust.edu.sa; casado@uma.es; webster@ntu.edu.sg

Notes

The authors declare no competing financial interest.

■ ACKNOWLEDGMENTS

J.W. acknowledges financial support from the BMRC-NMRC grant (no. 10/1/21/19/642), MOE Tier 2 grant (MOE2011-T2-2-130), and IMRE Core funding (IMRE/10-1P0509). The work at Yonsei University was supported by WCU (World Class University) programs (R32-2010-10217-0) and an AFSOR/APARD grant (no. FA2386-09-1-4092). K.-W.H. acknowledges financial support from KAUST. The work at the University of Málaga was supported by the Ministerio de Educación y Ciencia (MEC) of Spain and by FEDER funds (project CTQ2009-10098 and to the Junta de Andalucía for the research project PO9-4708). We thank Dr. Tan Geok-Kheng for crystallographic analysis.

■ REFERENCES

(1) (a) Rajca, A. *Chem. Rev.* **1994**, *94*, 871−893. (b) Morita, Y.; Suzuki, K.; Sato, S.; Takui, T. *Nat. Chem.* **2011**, *3*, 197−204. (c) Lambert, C. *Angew. Chem., Int. Ed.* **2011**, *50*, 1756−1758. (d) Sun, Z.; Wu, J. *J. Mater. Chem.* **2012**, *22*, 4151−4160. (e) Sun, Z.; Ye, Q.; Chi, C.; Wu, J. *Chem. Soc. Rev.* **2012**, in press, DOI: 10.1039/C2CS35211G.

(2) Iwamura, H.; Koga, N. *Acc. Chem. Res.* **1993**, *26*, 346−351.

(3) (a) Nakano, M.; Kishi, R.; Takebe, A.; Nate, M.; Takahashi, H.; Kubo, T.; Kamada, K.; Ohta, K.; Champagne, B.; Botek, E. *Comput. Lett.* **2007**, *3*, 333−338. (b) Nakano, M.; Kishi, R.; Ohta, S.; Takahashi, H.; Kubo, T.; Kamada, K.; Ohta, K.; Botek, E.; Champagne, B. *Phys. Rev. Lett.* **2007**, *99*, 033001. (c) Nakano, M.; Minami, T.; Yoneda, K.; Muhammad, S.; Kishi, R.; Shigeta, Y.; Kubo, T.; Rougier, L.; Champagne, B.; Kamada, K.; Ohta, K. *J. Phys. Chem. Lett.* **2011**, *2*, 1094−1101. (d) Yoneda, K.; Nakano, M.; Fukui, H.; Minami, T.; Shigeta, Y.; Kubo, T.; Botek, E.; Champagne, B. *ChemPhysChem* **2011**, *12*, 1697−1707.

(4) Kamada, K.; Ohta, K.; Kubo, T.; Shimizu, A.; Morita, Y.; Nakasuji, K.; Kishi, R.; Ohta, S.; Furukawa, S.; Takahashi, H.; Nakano, M. *Angew. Chem., Int. Ed.* **2007**, *46*, 3544−3546.

(5) Koide, T.; Furukawa, K.; Shinokubo, H.; Shin, J.-Y.; Kim, K. S.; Kim, D.-H.; Osuka, A. *J. Am. Chem. Soc.* **2010**, *132*, 7246−7247.

(6) (a) Pathenopoulos, D. A.; Rentzepis, P. M. *Science* **1989**, *245*, 843−845. (b) Zhou, W.; Kuebler, S. M.; Braun, K. L.; Yu, T.; Cammack, J. K.; Ober, C. K.; Perry, J. W.; Marder, S. R. *Science* **2002**, *296*, 1106−1109. (c) Pawlicki, M.; Collins, H. A.; Denning, R. G.; Anderson, H. L. *Angew. Chem., Int. Ed.* **2009**, *48*, 3244−3266. (d) Frederiksen, P. K.; Jøgensen, M.; Ogilby, P. R. *J. Am. Chem. Soc.* **2001**, *123*, 1215−1221.

(7) Chikamatsu, M.; Mikami, T.; Chisaka, J.; Yoshida, Y.; Azumi, R.; Yase, K. *Appl. Phys. Lett.* **2007**, *91*, 043506.

(8) Morita, Y.; Nishida, S.; Murata, T.; Moriguchi, M.; Ueda, A.; Satoh, M.; Arifuku, K.; Sato, K.; Takui, T. *Nat. Mater.* **2011**, *10*, 947−951.

(9) (a) Son, Y. W.; Cohen, M. L.; Louie, S. G. *Nature* **2006**, *444*, 347−349. (b) Son, Y. W.; Cohen, M. L.; Louie, S. G. *Phys. Rev. Lett.* **2006**, *97*, 216803. (c) Kim, W. Y.; Kim, K. S. *Nat. Nanotechnol.* **2008**, *3*, 408−412.

(10) (a) Kolc, J.; Michl, J. *J. Am. Chem. Soc.* **1970**, *92*, 4147−4148. (b) Iwashita, S.; Ohta, E.; Higuchi, H.; Kawai, H.; Fujiwara, K.; Ono, K.; Takenaka, M.; Suzuki, T. *Chem. Commun.* **2004**, 2076−2077. (c) Shimizu, A.; Tobe, Y. *Angew. Chem., Int. Ed.* **2011**, *50*, 6906−6910.

(11) (a) Thiele, J.; Balhorn, H. *Chem. Ber.* **1904**, *37*, 1463. (b) Flynn, C. R.; Michl, J. *J. Am. Chem. Soc.* **1974**, *96*, 3280−3288. (c) Chase, D. T.; Rose, B. D.; McClintock, S. P.; Zakharov, L. N.; Haley, M. M. *Angew. Chem., Int. Ed.* **2011**, *50*, 1127−1130.

(12) (a) Reid, D. H. *Chem. Ind.* **1956**, 1504−1505. (b) Gerson, F. *Helv. Chim. Acta* **1966**, *49*, 1463−1472. (c) Goto, K.; Kubo, T.; Yamamoto, K.; Nakasuji, K.; Sato, K.; Shiomi, D.; Takui, T.; Kubota, M.; Kobayashi, T.; Yakusi, K.; Ouyang, J.-Y. *J. Am. Chem. Soc.* **1999**, *121*, 1619−1620. (d) Itkis, M. E.; Chi, X.; Cordes, A. W.; Haddon, R. C. *Science* **2002**, *296*, 1443−1445.

(13) (a) Ohashi, K.; Kubo, T.; Masui, T.; Yamamoto, K.; Nakasuji, K.; Takui, T.; Kai, Y.; Murata, I. *J. Am. Chem. Soc.* **1998**, *120*, 2018−2027. (b) Kubo, T.; Sakamoto, M.; Akabane, M.; Fujiwara, Y.; Yamamoto, K.; Akita, M.; Inoue, K.; Takui, T.; Nakasuji, K. *Angew. Chem., Int. Ed.* **2004**, *43*, 7474−6479. (c) Kubo, T.; Shimizu, A.; Sakamoto, M.; Uruichi, M.; Yakushi, K.; Nakano, M.; Shiomi, D.; Sato, K.; Takui, T.; Morita, Y.; Nakasuji, K. *Angew. Chem., Int. Ed.* **2005**, *44*, 6564−6568. (d) Shimizu, A.; Uruichi, M.; Yakushi, K.; Matsuzaki, H.; Okamoto, H.; Nakano, M.; Hirao, Y.; Matsumoto, K.; Kurata, H.; Kubo, T. *Angew. Chem., Int. Ed.* **2009**, *48*, 5482−5486. (e) Shimizu, A.; Kubo, T.; Uruichi, M.; Yakushi, K.; Nakano, M.; Shiomi, D.; Sato, K.; Takui, T.; Hirao, Y.; Matsumoto, K.; Kurata, H.; Morita, Y.; Nakasuji, K. *J. Am. Chem. Soc.* **2010**, *132*, 14421−14428. (f) Shimizu, A.; Hirao, Y.; Matsumoto, K.; Kurata, H.; Kubo, T.; Uruichi, M.; Yakushi, K. *Chem. Commun.* **2012**, *48*, 5629−5631.

(14) Kubo, T.; Yamamoto, K.; Nakasuji, K.; Takui, T.; Murata, I. *Angew. Chem., Int. Ed. Engl.* **1996**, *35*, 439−441.

(15) Konishi, A.; Hirao, Y.; Nakano, M.; Shimizu, A.; Botek, E.; Champagne, B.; Shiomi, D.; Sato, K.; Takui, T.; Matsumoto, K.; Kurata, H.; Kubo, T. *J. Am. Chem. Soc.* **2010**, *132*, 11021−11023.

(16) (a) Sun, Z.; Huang, K.-W.; Wu, J. *J. Am. Chem. Soc.* **2011**, *133*, 11896−1199. (b) Li, Y.; Heng, W.-K.; Lee, B. S.; Aratani, N.; Zafra, J. L.; Lee, R.; Young, M. S.; Sun, Z.; Huang, K.-W.; Webster, R. D.;

Lopez Navarrette, J. T.; Kim, D.; Osuka, A.; Casado, J.; Ding, J.; Wu, J. *J. Am. Chem. Soc.* **2012**, DOI: 10.1021/ja304618v.

(17) (a) Chichibabin, A. E. *Chem. Ber.* **1907**, *40*, 1810. (b) Sloan, G. J.; Vaughan, W. R. *J. Org. Chem.* **1957**, *22*, 750−761. (c) Morozova, D. I.; Dyatkina, E. M. *Russ. Chem. Rev.* **1968**, *37*, 377−391. (d) Montgomery, L. K.; Huffman, J. C.; Jurczak, E. A.; Grendze, M. P. *J. Am. Chem. Soc.* **1986**, *108*, 6004−6011. (e) Porter, W. W., III; Vaid, T. P.; Rheingold, A. L. *J. Am. Chem. Soc.* **2005**, *127*, 16559−16566.

(18) (a) Bent, H. E.; Gould, R. G., Jr. *J. Am. Chem. Soc.* **1935**, *57*, 1217. (b) Platz, M. S. In *Diradical*; Borden, W. T., Ed.; Wiley: New York, 1982; pp 195−258. (c) McConnell, H. M. *J. Chem. Phys.* **1960**, *33*, 1868−1869.

(19) (a) Popp, F.; Bickelhaupt, F.; Maclean, C. *Chem. Phys. Lett.* **1978**, *55*, 327−330. (b) Sartorius, R.; Brauer, H.-D. *Angew. Chem., Int. Ed. Engl.* **1972**, *11*, 531−532.

(20) Ballester, M.; Pascual, I.; Carreras, C.; Vidal-Gancedo, J. *J. Am. Chem. Soc.* **1994**, *116*, 4205−4210.

(21) (a) Koelsch, C. F. *J. Am. Chem. Soc.* **1957**, *79*, 4439−4441. (b) Theilacker, W.; Schulz, H.; Baumgarte, U.; Drossier, H. G.; Rohde, W.; Thater, F.; Uffman, H. *Angew. Chem.* **1957**, *69*, 332. (c) Kuhn, R.; Neugebauer, F. A. *Monatsh. Chem.* **1964**, *95*, 322−333. (d) Ballester, M.; Riera-Figueras, J.; Castaner, J.; Badfa, C.; Monso, J. M. *J. Am. Chem. Soc.* **1971**, *93*, 2215−2225.

(22) (a) Mills, N. S.; Malandra, J. L.; Burns, E. E.; Green, A.; Unruh, K. E.; Kadlecek, D. E.; Lowery, J. A. *J. Org. Chem.* **1997**, *62*, 9318−9322. (b) Mills, N. S. *J. Am. Chem. Soc.* **1999**, *121*, 11690−11696. (c) Mills, N. S.; Benish, M. M.; Ybarra, C. *J. Org. Chem.* **2002**, *67*, 2003−2012. (d) Mills, N. S.; Tirla, C.; Benish, M. A.; Rakowitz, A. J.; Bebell, L. M.; Hurd, C. M. M.; Bria, A. L. M. *J. Org. Chem.* **2005**, *70*, 10709−10716. (e) Mills, N. S.; Llagostero, K. B.; Tirla, C.; Gordon, S.; Carpenetti, D. *J. Org. Chem.* **2006**, *71*, 7940−7946.

(23) (a) Clar, E. *Chem. Ber.* **1948**, *81*, 52−63. (b) Kuroda, H. *J. Chem. Soc.* **1960**, 1856−1857. (c) Arabei, S. M.; Pavich, T. A. *J. Appl. Spectrosc.* **2000**, *67*, 236−244.

(24) Zhang, K.; Huang, K.-W.; Li, J.; Luo, J.; Chi, C.; Wu, J. *Org. Lett.* **2009**, *11*, 4854−4857.

(25) Crystallographic data for **1-CS**: The asymmetric unit contains two molecules of $C_{35}H_{34}$ (**1-CS**) and three dichloromethane solvent, $C_{73}H_{74}Cl_6$. Triclinic, space group *P*-1; a = 11.7349(19) Å, b = 15.925(3) Å, c = 19.034(3) Å, α = 99.153(4)°, β = 103.775(4)°, γ = 105.180(3)°; V = 3239.8(9) Å^3; Z = 2; ρ_{calcd} = 1.193 Mg/m^3; R_1 = 0.1258 ($I > 2\sigma(I)$), wR_2 = 0.3605 (all data). The *t*-butyl group and the DMC had very large thermal parameters, indicating large thermal motion or loose packing. One of the *t*-butyl groups was treated as disorder to account for the thermal parameters. Restraints in bond distances were applied to the atoms of the *t*-butyl groups and the DCM. These restraints were applied so that the final refinement cycles can converge and result in reasonable bond geometry.

(26) Wu, J.; Pisula, W.; Müllen, K. *Chem. Rev.* **2007**, *107*, 718−747.

(27) (a) Zhai, L.; Shukla, R.; Rathore, R. *Org. Lett.* **2009**, *11*, 3437−3440. (b) Zhai, L.; Ruchi, S.; Shriya, H. W.; Rathore, R. *J. Org. Chem.* **2010**, *75*, 4748−4760. (c) Navale, T. S.; Thakur, K.; Rathore, R. *Org. Lett.* **2011**, *13*, 1634−1637.

(28) Yanai, T.; Tew, D.; Handy, N. *Chem. Phys. Lett.* **2004**, *393*, 51−57.

(29) Müller, U.; Baumgarten, M. *J. Am. Chem. Soc.* **1995**, *117*, 5840−5850.

(30) Teki, Y.; Miyamoto, S.; Nakatsuji, M.; Miura, Y. *J. Am. Chem. Soc.* **2001**, *123*, 294−305.

(31) Ikuhiro, N.; Masaki, S.; Tamejiro, H. *Angew. Chem., Int. Ed.* **2009**, *48*, 7573−7576.

(32) The electrolysis has been conducted for a long time (>1 week). However, 100% conversion was still not achievable. The separation of the cyclodehydrogenation product (possibly **1-CS-closed**) from the starting materials was not so successful at the moment because of their nearly same polarity on silica gel column. Further studies on the cyclodehydrogenation reaction of **1-CS** by electrochemical, chemical, and photochemical methods are underway in our laboratories.

(33) (a) Olah, G. A.; Schlosberg, R. H. *J. Am. Chem. Soc.* **1968**, *90*, 2726−2727. (b) Montgomery, L. K.; Huffman, J. C.; Jurczak, E. A.; Grendze, M. P. *J. Am. Chem. Soc.* **1986**, *108*, 6004−6011. (c) Malandra, J. L.; Mills, N. S.; Kadlecek, D. E.; Lowery, J. A. *J. Am. Chem. Soc.* **1994**, *116*, 11622−11623. (d) Dahl, B. J.; Mills, N. S. *J. Am. Chem. Soc.* **2008**, *130*, 10179−10186. (e) Piekarski, A. M.; Mills, N. S.; Yousef, A. *J. Am. Chem. Soc.* **2008**, *130*, 14883−14890.

(34) (a) Deno, N. C.; Jaruzelski, J. J.; Schriesheim, A. *J. Org. Chem.* **1954**, *19*, 155−167. (b) Deno, N. C.; Jaruzelski, J. J.; Schriesheim, A. *J. Am. Chem. Soc.* **1955**, *77*, 3044−3051. (c) Olah, G. A.; Prakash, G. K. S.; Liang, G.; Westerman, P. W.; Kunde, K.; Chandrasekhar, J.; Schleyer, P. v. R. *J. Am. Chem. Soc.* **1980**, *102*, 4485−4492.

(35) (a) Casado, J.; Patchkovskii, S.; Zgierski, M. Z.; Hermosilla, L.; Sieiro, C.; Moreno Oliva, M.; López Navarrete, J. T. *Angew. Chem., Int. Ed.* **2008**, *47*, 1443−1446. (b) Ortiz, R. P.; Casado, J.; Hernandez, V.; Navarrete, J. T. L.; Viruela, P. M.; Ortí, E.; Takimiya, K.; Otsubo, T. *Angew. Chem., Int. Ed.* **2007**, *46*, 9057−9061. (c) Ortiz, R. P.; Casado, J.; Rodríguez González, S.; Hernández, V.; Navarrete, J. T. L.; Viruela, P. M.; Ortí, E.; Takimiya, K.; Otsubo, T. *Chem.-Eur. J.* **2010**, *16*, 470−484. (d) Casado, J.; Navarrete, J. T. L. *Chem. Rec.* **2011**, *11*, 45−53.

(36) (a) Karpiuk, J.; Grabowskiv, Z. R. *Chem. Phys. Lett.* **1989**, *160*, 451−456. (b) Giacobbe, E. M.; Mi, G, Q.; Colvin, M. T.; Cohen, B.; Ramana, A.; Scott, A. M.; Yeganeh, S.; Marks, T. J.; Ratner, M. A.; Wasielewski, M. R. *J. Am. Chem. Soc.* **2009**, *131*, 3700−3712. (c) Colvin, M. T.; Smeigh, A. L.; Giacobbe, E. M.; Conron, S. M. M.; Ricks, A. B.; Wasielewski, M. R. *J. Phys. Chem. A* **2011**, *115*, 7538−7538. (d) Colvin, M. T.; Giacobbe, E. M.; Cohen, B.; Miura, T.; Scott, A. M.; Wasielewski, M. R. *J. Phys. Chem. A* **2010**, *114*, 1741−1748. (e) Ishii, K.; Hirose, Y.; Fujitsuka, H.; Ito, O.; Kobayashi, N. *J. Am. Chem. Soc.* **2001**, *123*, 702−708.

(37) Hui, Y.; Chng, E. L. K.; Chng, C. Y. L.; Poh, H. L.; Webster, R. D. *J. Am. Chem. Soc.* **2009**, *131*, 1523−1534.

(38) (a) Lee, C.; Yang, W.; Parr, R. G. *Phys. Rev. B* **1988**, *37*, 785−789. (b) Becke, A. D. *J. Chem. Phys.* **1993**, *98*, 5648−5652. (c) Ditchfie, R. W.; Hehre, J.; Pople, J. A. *J. Chem. Phys.* **1971**, *54*, 724−728. (d) Hehre, W. J.; Ditchfie, R.; Pople, J. A. *J. Chem. Phys.* **1972**, *56*, 2257−2261. (e) Harihara, P. C.; Pople, J. A. *Theor. Chim. Acta* **1973**, *28*, 213−222.